Air bubbles in calcium caseinate fibrous material enhances anisotropy

Wang, Zhaojun; Tian, Bei; Boom, Remko; van der Goot, Atze Jan

DOI
10.1016/j.foodhyd.2018.08.037

Publication date
2019

Document Version
Final published version

Published in
Food Hydrocolloids

Food Hydrocolloids 87 (2019) 497–505

Contents lists available at ScienceDirect

Food Hydrocolloids

journal homepage: www.elsevier.com/locate/foodhyd

Air bubbles in calcium caseinate fibrous material enhances anisotropy

Zhaojun Wang[a], Bei Tian[b], Remko Boom[a], Atze Jan van der Goot[a,*]

[a] Food Process Engineering, Wageningen University & Research, PO Box 17, 6700AA, Wageningen, the Netherlands
[b] Department of Radiation Science and Technology, Faculty of Applied Science, Delft University of Technology, Mekelweg 15, 2629JB, Delft, the Netherlands

ARTICLE INFO

Keywords:
Air bubble
Fibrous material
Microstructure
Mechanical property
Anisotropy

ABSTRACT

Dense calcium caseinate dispersions can be transformed into hierarchically fibrous structures by shear deformation. This transformation can be attributed to the intrinsic properties of calcium caseinate. Depending on the dispersion preparation method, a certain amount of air gets entrapped in the sheared protein matrix. Although anisotropy is obtained in the absence of entrapped air, the fibrous appearance and mechanical anisotropy of the calcium caseinate materials are more pronounced with dispersed air present. The presence of air induces the protein fibers to be arranged in microscale bundles, and the fracture strain and stress in the parallel direction are larger compared with the material without air. The effects can be understood from the alignment of the fibers in the parallel direction, providing strain energy dissipation. This study shows that creation of anisotropy is the result of interactions between multiple phases.

1. Introduction

A decade ago, an anisotropic calcium caseinate structure was created by a novel technique based on well-defined shear flow (Manski, van der Goot, & Boom, 2007b, 2007a), which is relevant for its structural resemblance to meat. Therefore, it has a potential to be a basis of new meat analogue products. The calcium caseinate dispersion was deformed by simple shear flow and concurrent crosslinking by transglutaminase. A typical fiber diameter of ~100–200 nm was observed with scanning electron microscopy (Manski et al., 2007b). The formation of this fibrous morphology was attributed to the aggregation of caseinate micelles, which have mildly attractive interactions due to the divalent calcium ions (Manski, van Riemsdijk, Boom, & van der Goot, 2007c). The aggregates are susceptible to aligning in the shear flow and simultaneously solidifying with transglutaminase. The presence of calcium ions was shown to be essential; the anisotropic structure could not be formed with sodium caseinate, and the formation of the fibrous structure was blocked by the addition of sodium triphosphate, which exchanges the divalent calcium ions bound to the protein with sodium ions (Grabowska, van der Goot, & Boom, 2012).

Dispersed air was observed in these calcium caseinate fibrous materials (Manski et al., 2007b; Manski, van der Zalm, van der Goot, & Boom, 2008), and also in materials created with soy protein isolate with wheat gluten blend (Grabowska, Tekidou, Boom, & van der Goot, 2014) and soy protein isolate with pectin blend (Dekkers, Hamoen, Boom, & van der Goot, 2018). A more recent study revealed that such fibrous materials may contain up to 20% (v/v) air with an average bubble diameter of ~100–400 μm (Tian, Wang, van der Goot, & Bouwman, 2018). The dispersed air provides an additional phase that influences the texture, microstructure, and functionality (Campbell & Mougeot, 1999; Zúñiga & Aguilera, 2009). During dough mixing, it was found that air entrapment affects the dough rheology. The rate of work input during dough mixing increased due to the presence of air bubbles while the resistance of dough to failure decreased under biaxial extension (Chin, Martin, & Campbell, 2005). A study on agar gel showed that an aerated gel is stronger than a gel without air (Ross, Pyrak-Nolte, & Campanella, 2006; Tiwari & Bhattacharya, 2011). Many natural porous composites, which are often hierarchically organized at multiple length scales (nano-, micro- and macroscale), have remarkable strength from the alignment of their fibers, crystals, or other structural elements, but have great toughness at low density (Gibson, 2012; Wegst, Bai, Saiz, Tomsia, & Ritchie, 2015); examples are bamboo and wood. The voids play a significant role in fracture toughening (Habibi & Lu, 2014; Lakes, 1993; Stanzl-Tschegg, Keunecke, & Tschegg, 2011; Wegst et al., 2015). For wood, the pores within the structure arrest cracks by the dispersion of stress over the surface of the pore after it has been compromised (Stanzl-Tschegg et al., 2011). This also occurs in synthetic cellular composite materials, such as honeycombs (Greil et al., 2002; Haghpanah, Oftadeh, Papadopoulos, & Vaziri, 2013) and foams (Andersons, Kirpluks, Stiebra, & Cabulis, 2015; Olurin, Fleck, & Ashby,

* Corresponding author.
E-mail addresses: zhaojun.wang@wur.nl (Z. Wang), B.Tian-1@tudelft.nl (B. Tian), remko.boom@wur.nl (R. Boom), atzejan.vandergoot@wur.nl (A.J. van der Goot).

https://doi.org/10.1016/j.foodhyd.2018.08.037
Received 23 May 2018; Received in revised form 20 August 2018; Accepted 20 August 2018
Available online 22 August 2018

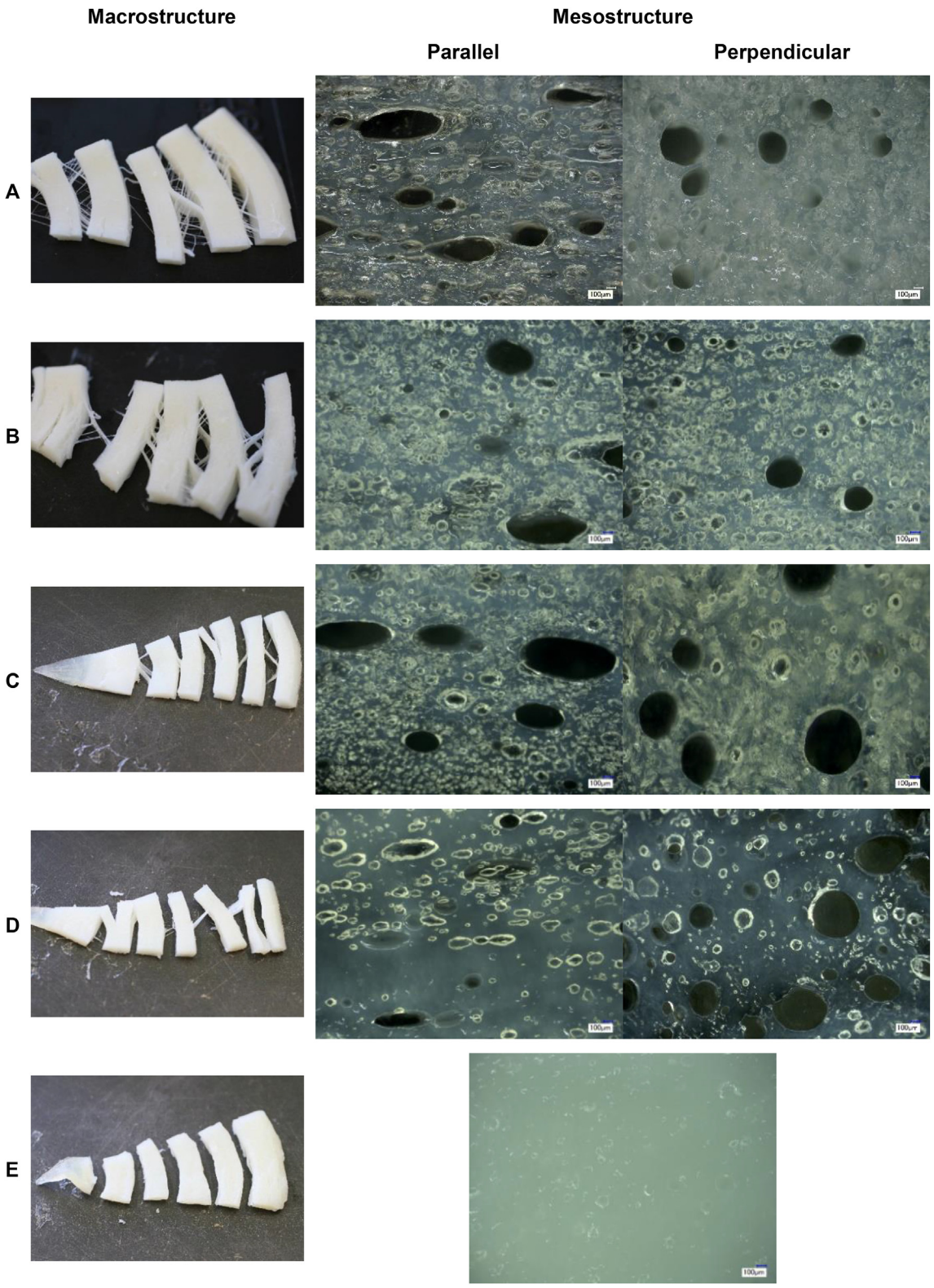

Fig. 1. Macrostructure and light microscopy images of 30% w/w calcium caseinate materials prepared with the different premixes A–E. The scale bars in the light microscopy images denote 100 μm.

2001).

The entrapment of air can introduce an extra separate phase into the calcium caseinate material (Manski et al., 2008), and may well lead to different mechanical properties. In this paper, we investigate the role of air bubbles on the microstructure and mechanical properties of the material structure. The morphology of entrapped air was studied with reflective light microscopy and X-ray tomography. Scanning electron microscopy was used to study the protein structure in the vicinity of air bubbles. Differences in mechanical properties were revealed with tensile analysis.

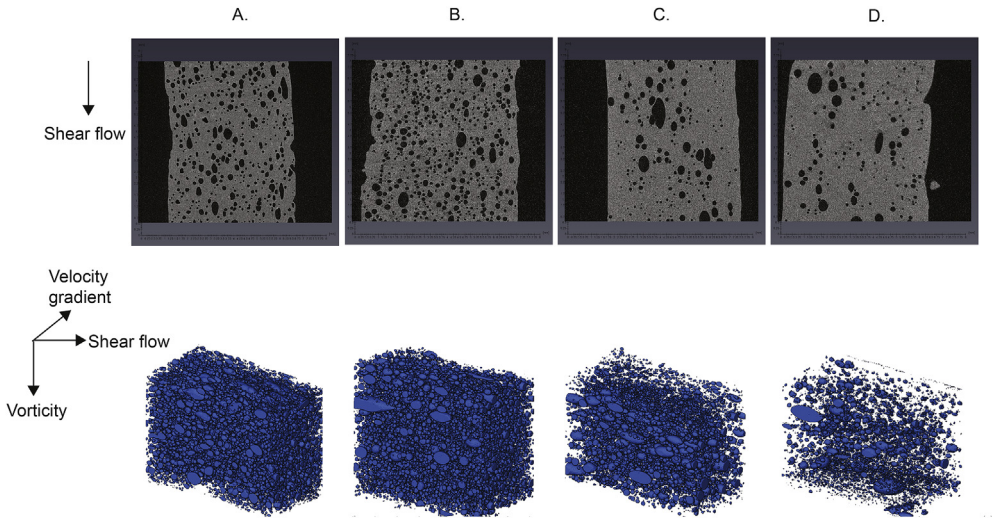

Fig. 2. X-ray tomography images of air bubble morphology in sheared calcium caseinate materials A–D. The blue color represents air bubble. (For interpretation of the references to color in this figure legend, the reader is referred to the Web version of this article.)

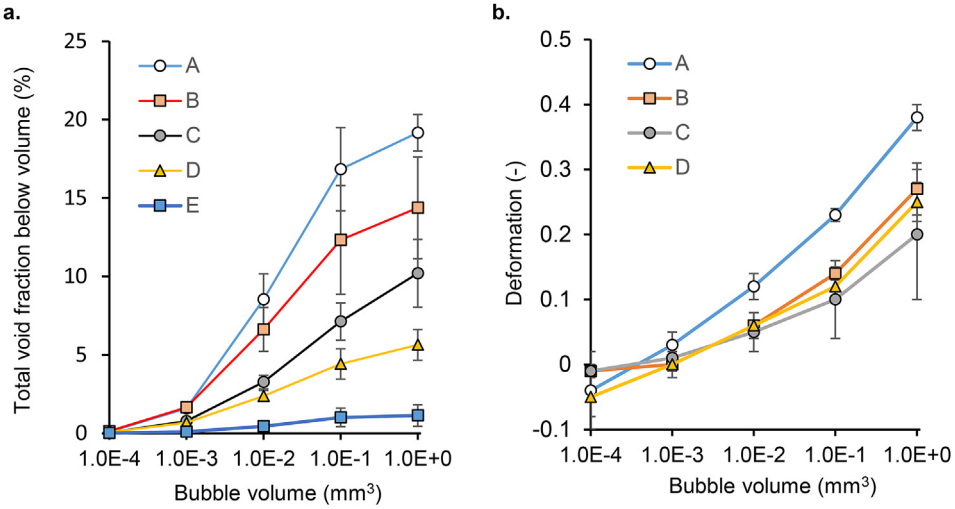

Fig. 3. a: Overall cumulative void fractions (as the void fraction below the bubble volume in mm^3). b: Associated deformation of the bubbles. The lines have been added to guide the eye.

2. Materials and methods

2.1. Materials

Spray-dried calcium caseinate was kindly provided by DMV International (Veghel, the Netherlands). The calcium caseinate powder contains 89 wt% protein and 1.5 wt% calcium according to the manufacturer's specifications. The activity of microbial Ca^{2+}-independent transglutaminase derived from *Streptoverticillium moberansae* (1% transglutaminase, 99% maltodextrine; Ajinomoto Co. Inc., Tokyo, Japan) was 114 units·g^{-1} as determined with the hydroxamate method (Yokoyama et al., 2003). This product was referred to as "enzyme" in this paper. A 20% (w/w in demineralized water) enzyme solution was stirred at room temperature for 1 h, and stored at 4 °C for 7 days before use (Grabowska et al., 2012).

2.2. Protein premixes for preparative shearing

Five protein premixes, referred to as premixes A–E, were prepared. All dispersions contained 30% (w/w) calcium caseinate powder, and transglutaminase was added to one of the dispersions. Premix A was prepared by manually mixing the protein, water and transglutaminase solution (enzyme-protein ratio 1:20) with a spatula for 1 min. The purpose of mixing was to roughly blend protein with water with minimal mixing intensity. Premix B was prepared similarly to premix A, but without the addition of transglutaminase solution. Premix C was prepared by manually mixing the protein and water with a spatula for 1 min, and then resting at room temperature for an additional 1 h. Premix D was prepared by manually mixing the protein and water with a spatula for 1 min, then heating the dispersion at 80 °C for 5 min and subsequently leaving it at room temperature for 55 min. Premix E was prepared similarly to premix D but an additional centrifugation step (2500 × *g* for 2 min) was used to remove most of the air from the mixture.

2.3. Sample preparation in the shear cell device

A shear device with gap angle 2.5° (Wageningen University, the Netherlands) was used to structure the dense calcium caseinate dispersions into anisotropic materials. The shear device is depicted and described in more detail by van der Zalm, Berghout, van der Goot, and Boom (2012). The rotating cone and the stationary cone were thermostatted with a heating and a cooling water bath. The premixes were transferred to the pre-heated (50 °C) shearing device. The materials

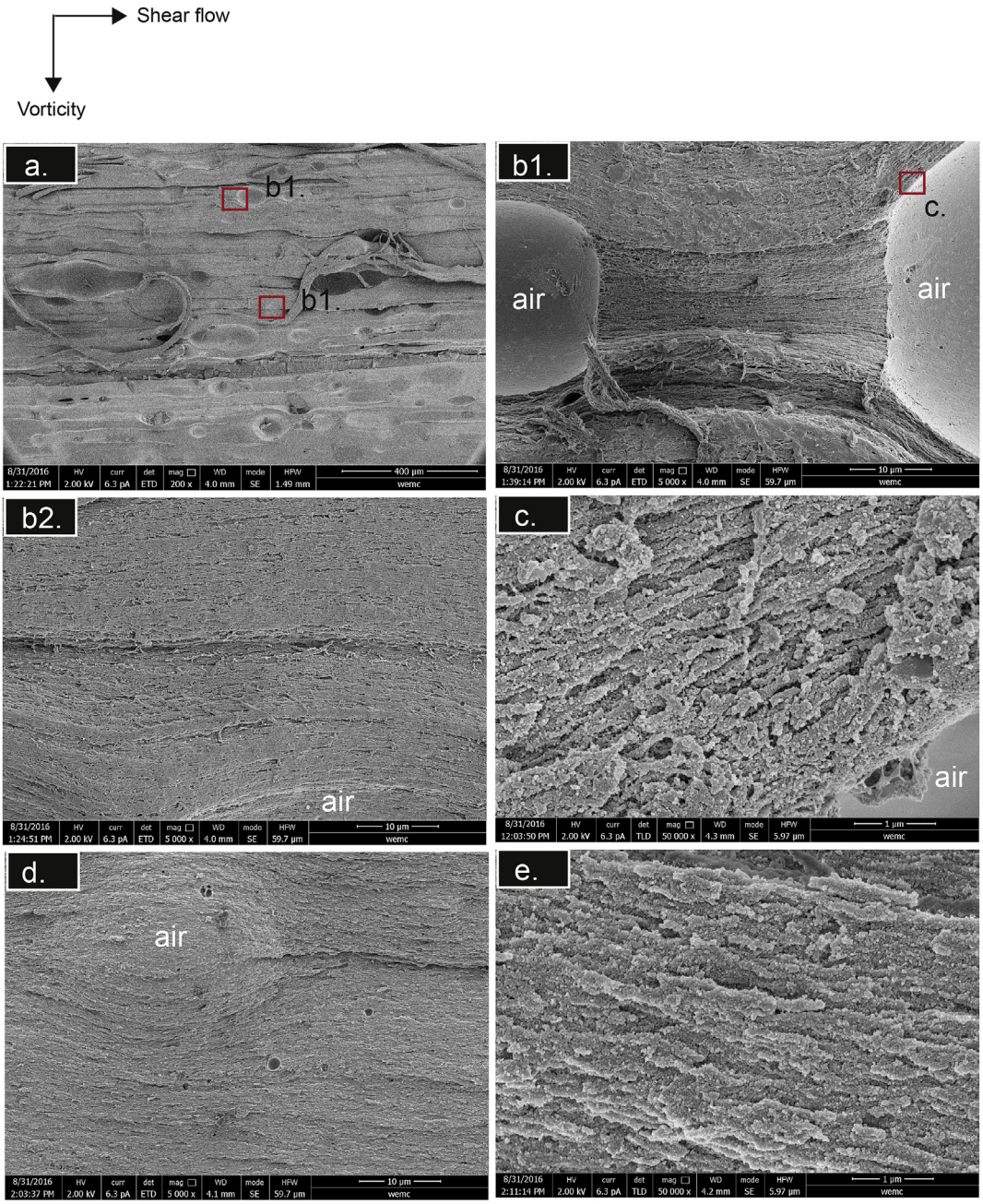

Fig. 4. SEM images of the fractured surface parallel to the shear flow of material A (images a–c) and B (images d–e). The scale bars denote 400 μm in image a, 10 μm in images b1, b2 and d, and 1 μm in images c and e. Images b1 and b2 zoom in on the area outlined by the red square in image a at 5000 × . Images in c zoom in on the area outlined by the red square in image b1 at 50 000 × . The air represents air bubbles in the images.

were made with a rotating speed of 50 rpm for 5 min at 50 °C. After processing, the materials were cooled to 4 °C in 10 min before removing them from the device. Tensile tests were performed on materials within 1 h after discharge from the device. Parts of the materials were stored at −20 °C until further analysis.

An extra experiment was done to elucidate the effect of air incorporation in the system and to exclude that the pretreatment influenced the structuring properties of the calcium caseinate. Premix E was whipped with a kitchen mixer (MUM54230/02, Bosch, Germany) at speed 6 (out of 7) for 5 min to again incorporate air in the premix before material preparation. The void fraction of the resulting material was 2.8 ± 0.2%. The resulting material showed similar mechanical properties and anisotropy as sample D (data not shown).

2.4. Tensile strength analysis

A texture analyzer (Instron Testing System, table model type 5564) was used with a load cell of 100 N. A tensile bar was used to take samples 15.2 mm long and 3.18 mm wide. The thickness of the samples varied between 4 and 6 mm. The samples were taken parallel and perpendicular to the shear flow (based on the shear-vorticity plane). The tensile tests were conducted at a constant deformation speed of 3 mm s−1. Grips with abrasive paper were used to prevent the sample slipping in the grips during testing. At least three specimens per direction were measured. The measurements were recorded using a camera in a smartphone. The results obtained from these tensile tests were depicted as force-displacement curves. The true stress (σ, kPa) and fracture strain (ε, –) were calculated using the following equations:

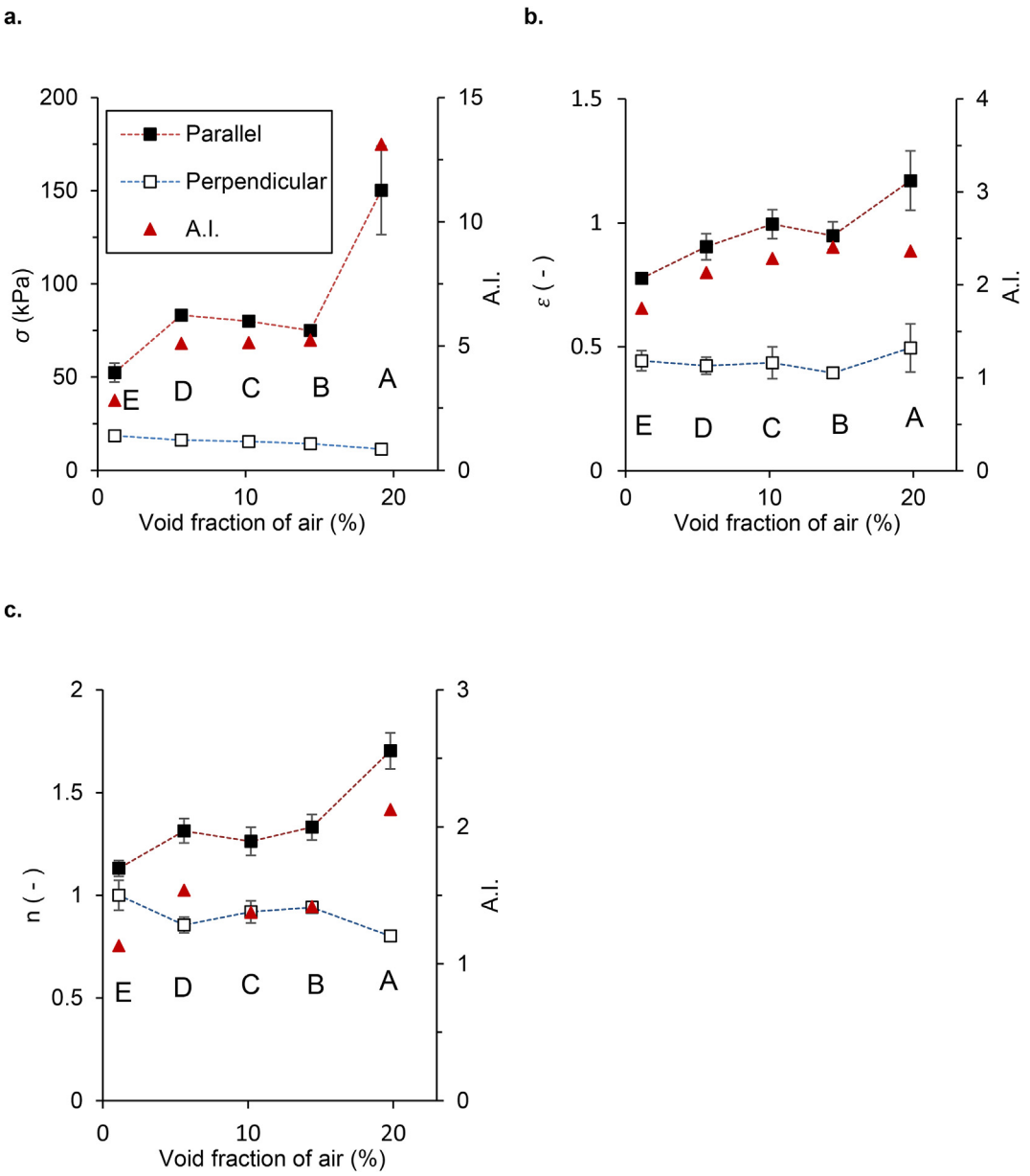

Fig. 5. Mechanical properties: (a) fracture stress σ, (b) fracture strain ε and (c) apparent strain hardening coefficient n as a function of void fraction of air for sheared 30% calcium caseinate materials A–E, deformed parallel (closed squares) and perpendicular (open squares) to the shear direction. The error bars for the mechanical properties are ± standard deviation; where not shown they were smaller than the marker used. The anisotropy index A.I. (red triangles) is ratio between the average data for the mechanical properties measured in the parallel and perpendicular directions to the shear flow. The lines have been added to guide the eye. (For interpretation of the references to color in this figure legend, the reader is referred to the Web version of this article.)

$$\sigma = F(t)/A(t)$$

$$\varepsilon = \ln(L(t)/L_0)$$

Where $F(t)$ was force, $A(t)$ was cross sectional area, and $L(t)$ was the length of the sample all at time t and L_0 was the initial length of the tensile bar (15.2 mm). A point following a dramatically decrease of stress in the stress-strain curve was taken as fracture point. This point was used to read fracture stress (σ, kPa) and fracture (Hencky) strain (ε, –), respectively. In this study, the apparent strain hardening coefficient n was calculated by applying a power law fit ($\sigma = k \cdot \varepsilon^{n}$) using the Hencky strain interval between 30% and 100% of fracture strain ε. When n exceeds 1, the sample exhibits strain hardening. k is a coefficient that correlates the stress and the stain of the materials and is therefore a measure of material stillness. The ratio of the average data for mechanical properties measured in the parallel and perpendicular directions to the shear flow was calculated and used as an indication of the mechanical anisotropy of the samples.

2.5. X-ray tomography

Samples were scanned using a GE Phoenix v|tome|x m tomographer (General Electric, Wunstorf, Germany) set at 80 kV/90 μA. The system contains two X-ray sources; the 240 kV micro-focus tube with a tungsten target was used. The images were recorded by a GE DXR detector array with 2024 × 2024 pixels (pixel size, 200 μm). The detector and object were located 815 mm and 28.55 mm from the X-ray source, respectively. This results in a spatial resolution of 7.00 μm. A full scan consists of 750 projections over 360°. Four images are taken for each projection. The first image was skipped; images 2–4 were averaged into one projection. GE reconstruction software (Wunstorf, Germany) was

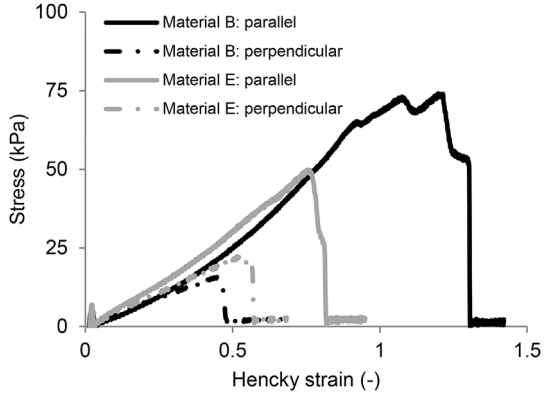

Fig. 6. Typical stress-strain curves of sheared 30% w/w calcium caseinate sample B (black) and sample E (grey) in the parallel (solid lines) and perpendicular direction (thick and thin lines) to the shear flow.

used to calculate the 3D structure via back projection. The 3D images were analyzed using Avizo imaging software version 9.3.0, including the total sample volume, total gas volume, gas void fraction (p), every single bubble volume, and its length, width and degree of deformation (Def). The degree of deformation (Def) was defined as:

$$Def = \frac{(a-b)}{(a+b)}$$

where a is the length of a deformed air bubble parallel to the shear flow, and b is the average width of the air bubble perpendicular to the shear flow (based on velocity gradient-shear flow plane and vorticity-shear flow plane). An average value of Def was used to represent the deformation of air bubble with different bubble volume range. Def = 0 represents a spherical air bubble; Def = 1 represents an infinitum deformed air bubble. Three samples of each materials were measured.

2.6. Scanning electron microscopy

The sheared calcium caseinate materials were torn apart by hand along the shear flow direction (approximately 2 mm, based on the shear flow-vorticity plane), and rinsed with demineralized water. Subsequently, the samples were fixated in a glutaraldehyde solution (2.5% v/v) for 1 h and dehydrated in a graded series of ethanol (10%, 30%, 50%, 70%, 90% and 100% v/v, 20 min each). Critical point drying with carbon dioxide (CPD 020, Balzers, Liechtenstein) was performed. The dried samples were then glued to sample holders using conductive carbon cement (Leit-C, Neubauer Chemicalien, Germany), and sputter coated with 15 nm platinum (JFC 1200, JEOL, Japan). The surface was observed with a field emission scanning electron microscope (Magellan 400, FEI, Eindhoven, the Netherlands) at ambient temperature at a working distance of 4–8 mm, with secondary electron detection at 2 kV and 6.3 pA.

2.7. Reflective light microscopy

The frozen materials were cut into thin slices with a razor blade (single-edge carbon steel; Electron Microscopy Sciences, Hatfiled, PA) parallel and perpendicular to the shear flow, resulting in the velocity gradient-shear flow plane and velocity gradient-vorticity plane, respectively. The samples were imaged using a digital microscope (Keyence VHX-2000E) with 100 × magnification.

3. Results and discussion

3.1. Macro- and microstructure

Fig. 1 shows the macrostructure of calcium caseinate materials A–E. A highly fibrous morphology was obtained when shearing a calcium caseinate premix with transglutaminase (material A). When this material was torn along the direction of shear flow, thin isolated fibers appeared, illustrating the pronounced fibrous character. Enzymatic crosslinking is not a prerequisite for the fibrous structure formation. Shearing 30% w/w calcium caseinate in the absence of transglutaminase (materials B–E) also gives anisotropy, but the materials are stickier than material A. Visual observation suggests that material E contains fewer isolated fibers than premixes B–D. Lack of air bubbles makes the material to break in larger parts, because the material contains hardly any air bubbles along which thin fibers can appear upon tearing.

Light microscopy (Fig. 1) shows that materials A-D contained many air bubbles. The larger and well-visible air bubbles were elongated and orientated in the direction parallel to the shear flow, which reveal that the presence of the air bubbles induced structural anisotropy at microscale. Small air bubbles were still circular due to their higher Laplace pressure. The image of material E shows the isotropic microstructure without air bubbles. We speculate that the presence of air bubble and fibrousness are correlated. The main explanation could be that the materials B-D break along the air bubble when tearing them along the direction of shear flow. Without air bubbles, structure will break into larger pieces upon tearing.

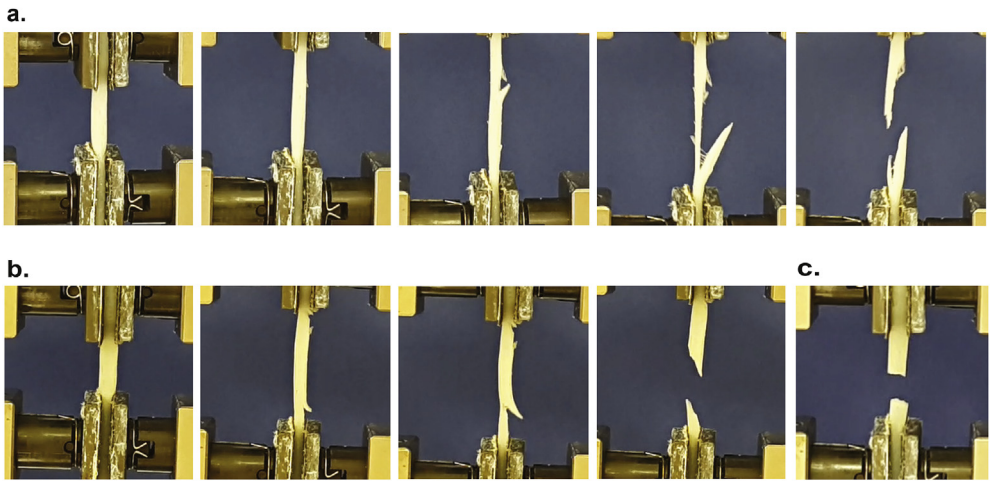

Fig. 7. Recorded images of a dog-bone specimen of samples B and E during the tensile test with a deformation rate of 3 mm s^{-1}. a: Sample B in the parallel direction. b: Sample E in the parallel direction. c: Sample E in the perpendicular direction to the shear flow.

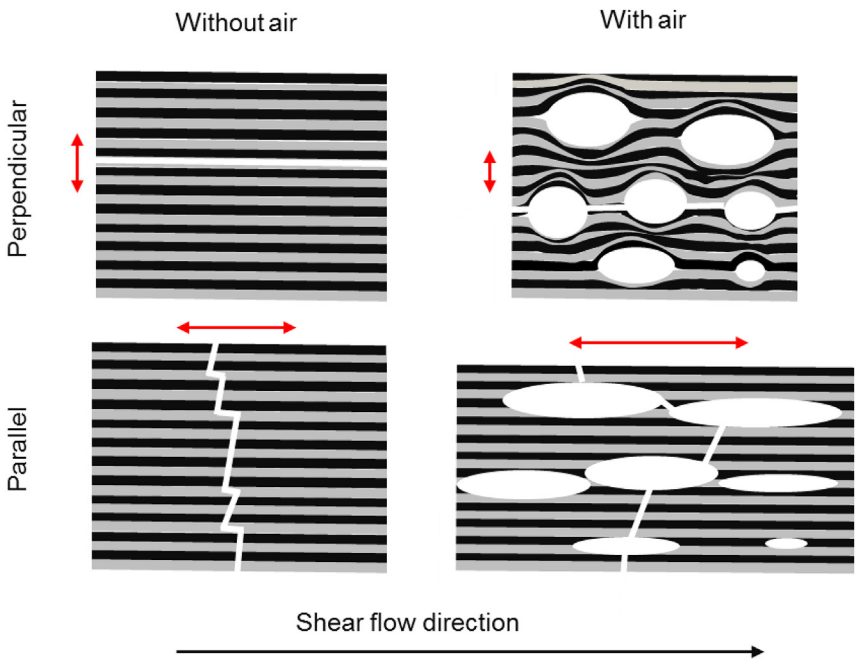

Fig. 8. Graphical illustration of the effect of air bubbles on the fracture behavior in sheared calcium caseinate material. The red arrows represent the direction of applied tensile force. The white ellipses represents the air bubbles in the material and the white lines represents the crack paths. The dark and grey lines represent the shear-induced protein alignments. (For interpretation of the references to color in this figure legend, the reader is referred to the Web version of this article.)

3.2. The morphology of air bubbles

2D and reconstructed 3D X-ray tomography images show the morphology of air bubbles in materials A–D (Fig. 2). These images confirmed the elongation and orientation of the air bubbles as illustrated in Fig. 1. It could be also deduced that the dispersed air bubbles could induce the fibers to be arranged in bundles at the microscale, thus yielding a hierarchical structure (Manski et al., 2008).

The reconstructed 3D images were used to determine the cumulative void fractions below different bubble volumes and the associated deformation of the bubbles (Fig. 3). The total void fraction decreased from material A to E, mainly due to the difference in the void fraction of large air bubbles ($> 10^{-3}\,mm^3$). Material A had a higher total void fraction of air (19.2 ± 1.2%) than material B (14.4 ± 3.2%), indicating that enzymatic crosslinking resulted in more air incorporation in the protein matrix. Going from material B to E, the void fraction of air decreased further. Apparently, more pretreatment (longer resting time and heating) of the premixes resulted in less air in the protein matrix. So far, it is not fully clear why heating and longer resting time reduced the void fractions. A possible explanation in case of heating is that a warmer dispersion has a lower viscosity, which enables escaping of air bubbles from the dispersion. Longer hydration also leads to a lower dispersion viscosity, because more interaction of calcium caseinate and water could lead to weakening of the dispersions. Besides, longer resting time also gives air bubbles more time to escape.

The deformation of air bubbles increased with increasing bubble volume in materials A–D (Fig. 3b). The small air bubbles ($\leq 10^{-3}\,mm^3$) were not deformed (−0.05–0.03), whereas the large air bubbles ($> 10^{-3}\,mm^3$) were slightly deformed (0.05–0.38). This is in line with the morphology of bubbles observed by light microscopy (Fig. 1). The deformation of the air bubbles was similar for materials B–D, however, material A showed larger deformation. This is probably due to the crosslinking in material A, resulting in a higher consistency during shearing and therefore larger force on the bubbles. In conclusion, the absence of transglutaminase reduced the air content and the degree of deformation.

3.3. Morphology around air bubbles

Fractured fibers on the microscale are visible parallel to the shear flow after tearing material A by hand along the shear flow direction (based on the shear-vorticity plane) (Fig. 4a). SEM images were obtained at different magnifications and locations close to air bubbles within this sample (Fig. 4b1,b2). The fiber alignment at the bubble surface more or less follows the curvature of a bubble (Fig. 4b1,b2). This is shown in more detail in Fig. 4c. The orientation of the fibers between two adjacent air bubbles follows the flow pattern around the bubbles (Fig. 4b1). In the absence of transglutaminase, the fiber orientation is still present (Fig. 4d and e.), but less distinct compared with material A (Fig. 4b and c).

3.4. Mechanical properties

The anisotropy index is the ratio of the fracture strain or stress parallel and perpendicular to the shear flow, which was used as an indication of the mechanical anisotropy of the sheared materials. Enzymatic crosslinking results in a high anisotropy for material A (Fig. 5). The main difference in materials B, C, and D is the void fraction of air; only a slight decrease in the anisotropy was found for those materials. Thus, the different pretreatments had little effect on their mechanical anisotropy. Material E showed only slight anisotropy. To conclude, the mechanical anisotropy increases when transglutaminase and air bubbles are present in calcium caseinate material.

Material A had the largest fracture stress and strain in the parallel direction and the smallest fracture stress in the perpendicular direction; the transglutaminase-induced crosslinking increases the strength in the parallel direction but not in the perpendicular direction, which is in line with previous research (Manski et al., 2007b). In the absence of transglutaminase, the fracture stress of materials B–D increased with decreasing void fraction of air in both the parallel and perpendicular directions. No significant differences were found in the fracture strain. The measurements show that material E, containing hardly any air, had the smallest fracture stress and strain in the direction parallel to shear flow. This indicates that the presence of air bubbles in the protein matrix reinforced the material in the parallel direction. In the perpendicular direction, all the materials become weaker with increased air content. In the perpendicular direction, air bubbles act as a weak phase, which promotes crack propagation along the fiber direction.

Fig. 5c showed strain hardening in the parallel direction but not in the perpendicular direction in all materials. A similar behavior was

reported by Bast et al. (2015) for mozzarella cheese and Grabowska et al. (2014) for an anisotropic soy-gluten structure. The strain hardening behavior in the calcium caseinate system became more pronounced when transglutaminase was added and air was incorporated. This strain hardening may be ascribed to the further alignment of the fibers around the bubbles, leading to an increase in strength. This only occurs in the parallel direction, not in the perpendicular direction. An increased crosslink density gives better adhesion between adjacent fibers and thus greater strength and better strain hardening (Kurtz, Pruitt, Jewett, Foulds, & Edidin, 1999). In the perpendicular direction, the fibers are just pulled apart. Here, the air bubbles work as a weak phase, similar to the role of the fat droplets in mozzarella cheese (Bast et al., 2015), which results in lower fracture strain and no strain hardening.

The sheared calcium caseinate material with entrapped air was more fibrous and exhibited larger anisotropy than the same material without air. We studied materials B and E further because these two have the largest and smallest void fraction and both were without transglutaminase (Figs. 6 and 7). In the parallel direction, material B reacts linearly elastic at small strains, followed by strain hardening and ultimately fluctuations close to the fracture point, indicating piecewise rupture of individual fibers or bundles of fibers. The strain hardening can be explained by further alignment of the fibers that are slightly misaligned due to the air bubbles. The fluctuating fracturing of material B is typical for fibrous composites, such as wood (Greil et al., 2002; Stanzl-Tschegg et al., 2011). Material E, having little air, exhibited only very minor strain hardening and relatively smooth breakage (Fig. 7b), indicative of a relatively brittle material. In the perpendicular direction, both materials break at relatively low stresses with smooth breakage (Figs. 6 and 7c).

3.5. Relationship between microstructure and mechanical properties

Fig. 8 interprets the influence of air bubbles in the matrix on the fracture behavior in different orientations (Gibson & Ashby, 1997; Greil, Lifka, & Kaindl, 1998). Based on the tensile tests, we postulate that air bubbles act as a weak phase in the perpendicular direction. The bubbles facilitate widening of a crack in between fibers, which then propagates along the orientation of fiber. In the parallel direction, the incorporated air misaligns the fibers somewhat. Pulling then results in a realignment of the fibers along the axis of the tensile stress, resulting in a net stronger material under stress. The local stress accumulation that may result from any incipient crack is distributed over the whole surface area of the air bubble, and therefore the stress concentration lessens and the material thus is tougher (Vincent, 2011). This relies on the existence of relatively strong fibers and the adhesion between the fibers which also determines the overall strength. This is evident by the fact that there is still some minor anisotropy at a void fraction close to zero. The porosity makes the material less susceptible to failure in the parallel direction, and more susceptible to breakage in the perpendicular direction, as is known for composite materials.

In the sheared calcium caseinate materials, the small air bubbles ($\leq 10^{-3}\,mm^3$) were not deformed (-0.05–0.03), whereas larger air bubbles ($> 10^{-3}\,mm^3$) were slightly deformed (0.05–0.38). When comparing the air bubbles incorporated in calcium caseinate with a previous study on fibrous materials from soy protein isolate-pectin (Dekkers et al., 2018), we noticed that calcium caseinate materials entrap more air bubbles, which are smaller in size and less deformed than in soy protein isolate-pectin blends (0.33–0.56). This may be due to the amphiphilic nature of caseinate. Smaller air bubbles have more surface area, therefore cause more local misalignment of the fibers, and thus will cause more strain hardening and arresting of cracks. Indeed, we see this strain hardening and tougher materials in the parallel direction with caseinate, but not with soy protein isolate-pectin blends.

4. Conclusion

Air incorporated in a calcium caseinate dispersion enhances the macroscopic and mechanical anisotropy of the fibrous morphology formed after shearing. Air bubbles can be considered as an additional phase that influences the local alignment of fibers. Air incorporation causes the material to become tougher with strain hardening in the direction parallel to the fibers, but makes the material somewhat more susceptible to fracture in the perpendicular direction. This insight can be used to design materials with the right degree of anisotropy, by allowing the right amount of air to be incorporated into the material.

Acknowledgements

The authors would like to thank the China Scholarship Council (grant number 201406820015) for financial support, Friesland Campina for kindly supplying the protein ingredients, Marlies Nijemeisland from Delft University of Technology for helping with the light microscope images, Remco Hamoen for X-ray tomography and Jarno Gieteling for technical support.

Appendix A. Supplementary data

Supplementary data related to this article can be found at https://doi.org/10.1016/j.foodhyd.2018.08.037.

References

Andersons, J., Kirpluks, M., Stiebra, L., & Cabulis, U. (2015). The effect of a circular hole on the tensile strength of neat and filled rigid PUR foams. *Theoretical and Applied Fracture Mechanics, 78*, 8–14. http://doi.org/https://doi.org/10.1016/j.tafmec.2015.05.001.

Bast, R., Sharma, P., Easton, H. K. B., Dessev, T. T., Lad, M., & Munro, P. A. (2015). Tensile testing to quantitate the anisotropy and strain hardening of mozzarella cheese. *International Dairy Journal, 44*, 6–14.

Campbell, G. M., & Mougeot, E. (1999). Creation and characterisation of aerated food products. *Trends in Food Science & Technology, 10*(9), 283–296. http://doi.org/10.1016/S0924-2244(00)00008-X.

Chin, N. L., Martin, P. J., & Campbell, G. M. (2005). Dough aeration and rheology: Part 3. Effect of the presence of gas bubbles in bread dough on measured bulk rheology and work input rate. *Journal of the Science of Food and Agriculture, 85*(13), 2203–2212. http://doi.org/10.1002/jsfa.2238.

Dekkers, B. L., Hamoen, R., Boom, R. M., & van der Goot, A. J. (2018). Understanding fiber formation in a concentrated SPI-pectin blend. *Journal of Food Engineering, 222*, 1–20. http://doi.org/10.1016/j.jfoodeng.2017.11.014.

Gibson, L. J. (2012). The hierarchical structure and mechanics of plant materials. *Journal of The Royal Society Interface, 9*(76), 2749–2766. http://doi.org/10.1098/rsif.2012.0341.

Gibson, L. J., & Ashby, M. F. (1997). *Cellular solids: Structure and properties* (2nd ed.). Cambridge: Cambridge University Press.

Grabowska, K. J., Tekidou, S., Boom, R. M., & van der Goot, A.-J. (2014). Shear structuring as a new method to make anisotropic structures from soy–gluten blends. *Food Research International, 64*, 743–751.

Grabowska, K. J., van der Goot, A. J., & Boom, R. M. (2012). Salt-modulated structure formation in a dense calcium caseinate system. *Food Hydrocolloids, 29*(1), 42–47.

Greil, P., Lifka, T., & Kaindl, A. (1998). Biomorphic cellular silicon carbide ceramics from wood: II. Mechanical properties. *Journal of the European Ceramic Society, 18*(14), 1975–1983. http://doi.org/https://doi.org/10.1016/S0955-2219(98)00155-1.

Greil, P., Vogli, E., Fey, T., Bezold, A., Popovska, N., Gerhard, H., et al. (2002). Effect of microstructure on the fracture behavior of biomorphous silicon carbide ceramics. *Journal of the European Ceramic Society, 22*(14–15), 2697–2707. http://doi.org/10.1016/S0955-2219(02)00135-8.

Habibi, M. K., & Lu, Y. (2014). Crack propagation in bamboo's hierarchical cellular structure. *Scientific Reports, 4*http://doi.org/10.1038/srep05598.

Haghpanah, B., Oftadeh, R., Papadopoulos, J., & Vaziri, A. (2013). Self-similar hierarchical honeycombs. *Proceedings of the Royal Society A, 469*, 2156.

Kurtz, S. M., Pruitt, L. A., Jewett, C. W., Foulds, J. R., & Edidin, A. A. (1999). Radiation and chemical crosslinking promote strain hardening behavior and molecular alignment in ultra-high molecular weight polyethylene during multi-axial loading conditions. *Biomaterials, 20*(16), 1449–1462.

Lakes, R. (1993). Materials with structural hierarchy. *Nature, 361*(6412), 511–515. http://doi.org/10.1038/361511a0.

Manski, J. M., van Riemsdijk, L. E., Boom, R. M., & van der Goot, A. J. (2007c). Importance of intrinsic properties of dense caseinate dispersions for structure formation. *Biomacromolecules, 8*(11), 3540–3547.

Manski, J. M., van der Goot, A. J., & Boom, R. M. (2007a). Advances in structure formation of anisotropic protein-rich foods through novel processing concepts. *Trends in*

Food Science & Technology, 18(11), 546–557.
Manski, J. M., van der Goot, A. J., & Boom, R. M. (2007b). Formation of fibrous materials from dense calcium caseinate dispersions. *Biomacromolecules, 8*(4), 1271–1279.
Manski, J. M., van der Zalm, E. E. J., van der Goot, A. J., & Boom, R. M. (2008). Influence of process parameters on formation of fibrous materials from dense calcium caseinate dispersions and fat. *Food Hydrocolloids, 22*(4), 587–600.
Olurin, O. B., Fleck, N. A., & Ashby, M. F. (2001). Tensile and compressive failure of notched cellular foams. *Advanced Engineering Materials, 3*(1–2), 55–58.
Ross, K. A., Pyrak-Nolte, L. J., & Campanella, O. H. (2006). The effect of mixing conditions on the material properties of an agar gel - microstructural and macrostructural considerations. *Food Hydrocolloids, 20*(1), 79–87. http://doi.org/10.1016/j.foodhyd.2005.01.007.
Stanzl-Tschegg, S. E., Keunecke, D., & Tschegg, E. K. (2011). Fracture tolerance of reaction wood (yew and spruce wood in the TR crack propagation system). *Journal of the Mechanical Behavior of Biomedical Materials, 4*(5), 688–698. http://doi.org/10.1016/j.jmbbm.2010.11.010.
Tian, B., Wang, Z., van der Goot, A. J., & Bouwman, W. G. (2018). Air bubbles in fibrous caseinate gels investigated by neutron refraction, X-ray tomography and refractive microscope. *Food Hydrocolloids, 83*, 287–295. http://doi.org/10.1016/j.foodhyd.2018.05.006.
Tiwari, S., & Bhattacharya, S. (2011). Aeration of model gels: Rheological characteristics of gellan and agar gels. *Journal of Food Engineering, 107*(1), 134–139. http://doi.org/https://doi.org/10.1016/j.jfoodeng.2011.05.036.
Vincent, J. F. V. (2011). Unusual uses of holes—with input from biology. *Journal of the Mechanical Behavior of Biomedical Materials, 4*(5), 682–687. http://doi.org/https://doi.org/10.1016/j.jmbbm.2010.10.002.
Wegst, U. G. K., Bai, H., Saiz, E., Tomsia, A. P., & Ritchie, R. O. (2015). Bioinspired structural materials. *Nature Materials, 14*(1), 23–36. http://doi.org/10.1038/nmat4089.
Yokoyama, K., Ohtsuka, T., Kuraishi, C., Ono, K., Kita, Y., Arakawa, T., et al. (2003). Gelation of food protein induced by recombinant microbial transglutaminase. *Journal of Food Science, 68*(1), 48–51. http://doi.org/10.1111/j.1365-2621.2003.tb14112.x.
van der Zalm, E. E. J., Berghout, J. A. M., van der Goot, A. J., & Boom, R. M. (2012). Starch–gluten separation by shearing: Influence of the device geometry. *Chemical Engineering Science, 73*, 421–430. http://doi.org/https://doi.org/10.1016/j.ces.2012.02.009.
Zúñiga, R. N., & Aguilera, J. M. (2009). Structure–fracture relationships in gas-filled gelatin gels. *Food Hydrocolloids, 23*(5), 1351–1357. http://doi.org/https://doi.org/10.1016/j.foodhyd.2008.11.012.